

Retraction

Retracted: To Improve the Real-Time Performance of Airborne Data Link Communication System

Mathematical Problems in Engineering

Received 18 July 2023; Accepted 18 July 2023; Published 19 July 2023

Copyright © 2023 Mathematical Problems in Engineering. This is an open access article distributed under the Creative Commons Attribution License, which permits unrestricted use, distribution, and reproduction in any medium, provided the original work is properly cited.

This article has been retracted by Hindawi following an investigation undertaken by the publisher [1]. This investigation has uncovered evidence of one or more of the following indicators of systematic manipulation of the publication process:

- (1) Discrepancies in scope
- (2) Discrepancies in the description of the research reported
- (3) Discrepancies between the availability of data and the research described
- (4) Inappropriate citations
- (5) Incoherent, meaningless and/or irrelevant content included in the article
- (6) Peer-review manipulation

The presence of these indicators undermines our confidence in the integrity of the article's content and we cannot, therefore, vouch for its reliability. Please note that this notice is intended solely to alert readers that the content of this article is unreliable. We have not investigated whether authors were aware of or involved in the systematic manipulation of the publication process.

Wiley and Hindawi regrets that the usual quality checks did not identify these issues before publication and have since put additional measures in place to safeguard research integrity.

We wish to credit our own Research Integrity and Research Publishing teams and anonymous and named external researchers and research integrity experts for contributing to this investigation.

The corresponding author, as the representative of all authors, has been given the opportunity to register their agreement or disagreement to this retraction. We have kept a record of any response received.

References

- [1] G. Yao, "To Improve the Real-Time Performance of Airborne Data Link Communication System," *Mathematical Problems in Engineering*, vol. 2021, Article ID 5558089, 11 pages, 2021.

Research Article

To Improve the Real-Time Performance of Airborne Data Link Communication System

Gang Yao 

School of Automation, Northwestern Polytechnical University, Xi'an 710072, Shaanxi, China

Correspondence should be addressed to Gang Yao; yao_gang@mail.nwpu.edu.cn

Received 7 January 2021; Revised 3 February 2021; Accepted 15 February 2021; Published 23 February 2021

Academic Editor: Sang-Bing Tsai

Copyright © 2021 Gang Yao. This is an open access article distributed under the Creative Commons Attribution License, which permits unrestricted use, distribution, and reproduction in any medium, provided the original work is properly cited.

Ground-to-air data link communication has the advantages of fast transmission rate, strong anti-interference ability, and large data communication volume and has been widely used in the field of civil aviation. This article mainly studies the measures to improve the real-time performance of the airborne data link communication system. The design of the hardware platform of the jamming environment simulator needs to comprehensively consider the implementation complexity of the jamming environment model and the real-time simulation method adopted by the UAV data link system. This paper uses the multicore and multithread in the Linux operating system to simulate the functions of the original data link communication system and uses the TFT screen to display the data communication process in the multicore and multithread design scheme. When evaluating and scoring the evaluation indicators, it must be carried out in accordance with certain standards. However, most of the indicators cannot be directly assessed quantitatively only through certain specific values. This article mainly uses the AHP method to analyze the weight of indicators. In the simulation, user information is generated by a random code generator and then distributed to each branch through serial-to-parallel conversion (S/P), and the spreading process is completed by long-code spreading on each branch, respectively, by BPSK. It is modulated on different carriers to form a transmission signal; the signal passes through a Gaussian white noise channel, and a certain frequency offset noise is added at the same time to reach the receiving end; the receiving end uses correlated demodulation, and after despreading, the error rate is counted. The data shows that under different distances, the frame loss rate of the data link is different. The frame loss rate in the 500 m range is about 1%, and the frame loss rate in the 2 km range is about 2.3%. The results show that the real-time performance of the data link communication system in this paper has been greatly improved.

1. Introduction

With the popularization and application of information theory, data link technology has evolved from traditional combat support to main combat weapons and has been proved in many wars since the 1990s. Compared with traditional wireless communication, there are many scenarios in which a wireless communication base station is used [1]. It can not only realize real-time communication in closed buildings such as rooms and parking lots but also realize real-time communication in the streets with high-rise buildings. This is of great significance for the development of wireless communication base stations.

UAV downlink data link not only solves the problems of long time [2], low timeliness, and instability of traditional

relay communication but also ensures the accuracy and integrity of the received information to the greatest extent due to its mobility and flexibility and further improves the processing capacity of the whole system for docking and receiving information. Whether the communication can be carried out at high speed, timely, correctly, and safely is the key factor affecting the success of the task. Therefore, the simulation research of UAV airborne communication system has great military practical significance [3].

For wireless communication in an open space, it is bound to be subject to various interferences from the open space. Long et al. reexamined the channel characteristics of indoor visible light communication systems. His purpose is to evaluate channel frequency selectivity, in other words, to evaluate the importance of intersymbol interference (ISI) at

the receiver and the need for channel equalization to restore the transmitted data. He focused on the effect of indoor channels by assuming that there is no bandwidth limitation on light-emitting diodes and considering a simple intensity modulation technique (not including discrete multitone modulation). First, he simulated the channel impulse response (CIR) using an iterative site-based method. Then, he studied the conventional indicators used to evaluate channel frequency selectivity, namely, root mean square delay spread and channel frequency response. Although his algorithm is necessary, it lacks accuracy [4]. Rahmani Hosseinabadi et al. proposed an efficient partial transmission sequence technology based on genetic algorithm and peak optimization algorithm (gapoa) to reduce the peak-to-average power ratio (PAPR) in the visible light communication system based on orthogonal frequency division multiplexing (vlc-ofdm). By analyzing the advantages and disadvantages of the mountain climbing algorithm [5], he proposed a kind of Poa with excellent local searchability, which can further process the signal whose PAPR still exceeds the threshold after being processed by genetic algorithm (GA). He evaluated the PAPR performance and bit error rate (BER) performance, compared them with ga-pts and genetic-based PTS, and compared them with gh-pts and sflahc-pts [6]. Although his research performance is better, the factors considered are not comprehensive [7]. Thakur P believes that, recently, due to the explosive growth of application requirements for bandwidth, the demand for the radio spectrum of the next-generation communication system continues to increase, which has caused the problem of spectrum scarcity. Among the proposed solutions to this problem, he uses the well-researched cognitive radio (CR) technology and the recently introduced nonorthogonal multiple access (NOMA) technology. Both technologies are used to effectively use the spectrum and ensure a significant increase in spectrum efficiency [8]. He introduced the framework for implementing NOMA on CR and the feasibility of the proposed framework. In addition, he discussed the differences between the proposed CR-NOMA and the conventional CR framework. Finally, he discussed potential issues regarding CR-NOMA's implementation. Although his research has certain feasibility, it lacks necessary data [9]. Kaddoum considers that the decrease of data rate and energy efficiency caused by the transmission of an equal reference signal and data carrier signal constitutes the main disadvantage of the DCSK system. In order to overcome this main shortcoming, he proposed a short reference DCSK system (SR-DCSK). To construct the transmitted data signal, P tandem copies of R are used to extend the data. This operation improves data rates and energy efficiency without adding complexity to the system architecture. He uses the receiver's knowledge of integers R and P to recover data. He analyzed the proposed system and calculated the enhanced data rate and bit energy saving percentage. Although his research enhanced the data rate, it was not accurate enough [10].

In this paper, the Turbo code is selected as the error-correcting code for the airborne data chain in consideration of hardware resources, feasibility, anti-interference ability, and other aspects, the Turbo code scheme is improved, and

finally, FPGA implementation is implemented. It plays a very important role in the communication system. The research on the information coding technology of airborne data link lays a certain foundation for the design of the message frame format, transmission mode, and signal processing method of the new airborne data link and verifies its effectiveness through the computer simulation, which provides a reference basis and technical support for the formulation of the message standard of the new airborne data link.

2. Airborne Data Link Communication System

2.1. Airborne Data Link. The terminal of the wireless data link, no matter it is a source or a host, is equivalent to a microcomputer, which has the ability to process information independently and can complete the modulation and demodulation function of transmitting the information. Moreover, according to the specified communication protocol, the demodulated information can be processed by group frames, and the true meaning of information transmission can be read out to achieve the purpose of communication [11]. On the other hand, the terminal equipment can also modulate the information to be expressed according to the communication protocol and then transmit it in the channel to complete the information feedback. As for the transmission channel of wireless data link, it covers a wider range, including not only transmission media but also some other devices, such as antenna [12]. In the data link communication system of a small unmanned helicopter [13], when the information load between UAV and ground station is too large, the throughput of the network will decrease, resulting in congestion. The expression of congestion detection function is as follows:

$$\rho = \frac{(\eta \times l_{\text{before}} + (1 - \eta) \times l_{\text{now}})}{q} \quad (1)$$

In the formula, q is the queue space. The formula for calculating the received power P_r of the receiving node is

$$Pr = P_0 + A_m + H_b + H_m + K_T. \quad (2)$$

In the automatic power control strategy, it is assumed that the energy consumption parameter α is

$$\alpha = \frac{e_r(k)}{e_0(k)}. \quad (3)$$

In general, when $k > 1$, the equivalent radius of the Earth is larger than the actual radius. For the same antenna and aircraft height, atmospheric refraction means that the communication distance of the data link increases, and the equivalent radius coefficient K of standard refraction is 1.333. The limit distance of line-of-sight propagation is

$$d_{(Km)} = 4.12 \left(\sqrt{h_{1(m)}} + \sqrt{h_{2(m)}} \right). \quad (4)$$

During the flight, the distance between the aircraft and the ground control station is constantly changing, and it may appear at any point within the line-of-sight range.

Compared with the receiver, the received signal will only be very close when it is very close to the signal source [14]. On the contrary, the farther the distance is, the worse the signal

will be, and this change is not a simple linear change. When it exceeds a certain distance, the signal strength will drop sharply [15, 16]. The form of the uplink modulation signal is

$$S_{\text{up}}(t) = \sqrt{2P_{\text{Iup}}}d_{\text{TCup}} \cos(2\pi f_{\text{up}}t) - \sqrt{2P_{\text{Qup}}}d_{\text{IMGup}}(t)c_{\text{IMGup}} \sin(2\pi f_{\text{up}}t). \quad (5)$$

In the formula, $c_{\text{IMGup}}(t)$ represents the pseudocode of the uplink communication branch, and f_{up} represents the uplink carrier frequency.

The downlink modulation signal form is

$$S_{\text{dn}}(t) = \sqrt{2P_{\text{TMdn}}}d_{\text{TM}}(t)c_{\text{TMdn}} \cos(2\pi f_{\text{dn}}t) - \sqrt{2P_{\text{MIMGdn}}}d_{\text{MIMGdn}}(t)\sin[2\pi(f_{\text{dn}} \pm \Delta f_1)t]. \quad (6)$$

In the formula, Δf_1 is the frequency difference between the target image branch and the telemetry branch [17, 18].

Assuming that the coordinates of the ground station are (x_0, y_0, z_0) and the coordinates of the aircraft are (x_i, y_i, z_i) , then

$$\begin{aligned} (D^2 - h^2)\cos^2 \theta &= (x_i - x_0)^2, \\ (D^2 - h^2)\sin^2 \theta &= (y_i - y_0)^2. \end{aligned} \quad (7)$$

Then the aircraft coordinates can be obtained:

$$\begin{aligned} x_i &= x_0 + \sqrt{(D^2 - h^2)} \cos \theta, \\ y_i &= y_0 + \sqrt{(D^2 - h^2)} \sin \theta, \\ z_i &= z_0 + h. \end{aligned} \quad (8)$$

At present, the M sequence is obtained through large-scale search and detailed calculation. Using the form of feedback function, the M sequence can be expressed as

$$f(x_1, x_2, \dots, x_k) = x_1 + f_1(x_1, x_2, \dots, x_k). \quad (9)$$

The autocorrelation function of the commonly used Barker code can be expressed as

$$\rho(t) = \sum_{k=1}^{n-t} x_k x_{k+t} = \begin{cases} n, & t = 0, \\ 0 \text{ or } \pm 1, & 0 < t < n, \\ 0, & t \geq n. \end{cases} \quad (10)$$

In the AWGN channel, the receiving sequence is

$$r(n) = s(n)e^{j2\pi f_e nT + j\theta} + w(n). \quad (11)$$

Among them, $w(n)$ is additive white Gaussian noise, and T is the symbol interval. Then, the ML probability is

$$\Lambda(f_e) = - \sum_{n=0}^{N-1} |r(n) - s(n)e^{j2\pi f_e nT + j\theta}|^2. \quad (12)$$

The carrier insertion method system is shown in Figure 1. At the receiving end of the communication system, the carrier frequency transmitted by the system can be filtered out by

using a narrow-band filter. Here, it is necessary to ensure that the center frequency of the narrow-band filter is the same as the inserted carrier frequency. At the same time, due to the orthogonal effect, the phase shift $\pi/2$ operation is also required [19]. In a word, the key of the carrier insertion method is a narrow-band filter with the same carrier frequency, which is usually completed by PLL, and its hardware implementation is [20–22].

2.2. Communication System. In order to improve the confidentiality and security of the data link communication process, it is necessary to deeply study the confidentiality of various communication systems [23]. In order to suppress the adjacent channel interference generated by the transmitting end, a filter with a high Q value is adopted before the power amplifier rear stage of the transmitting end to filter the stray signals from the orthogonal modulation circuit and prevent the interference to the receiving end caused by amplifier amplification [24]. At the same time, in order to realize full-duplex work, a pair of a machine is designed to isolate the transmitting signal and the receiving signal, so as to prevent the large signal of the transmitting end from interfering with the receiving end [25]. Cooperative engagement capability data link with other data chain's biggest difference is the cooperative engagement capability, and conventional data link is only in view of the target track, speed grades, and tracking accuracy of information processing [26].

2.3. System Real Time. If the transmission rate is too fast, it is easy to affect the communication performance. Therefore, in order to study the relationship between transmission rate and bit error rate, the relationship between transmission rate and signal-to-noise ratio is established by taking the signal-to-noise ratio as a bridge, so as to evaluate the link bit error performance [27]. The data to be transmitted is sent to the fountain code encoder to code the transmitted data, then the pilot sequence is added according to the specified data frame structure, and the information is grouped. The grouped data is modulated by QPSK. Before transmission, the data is

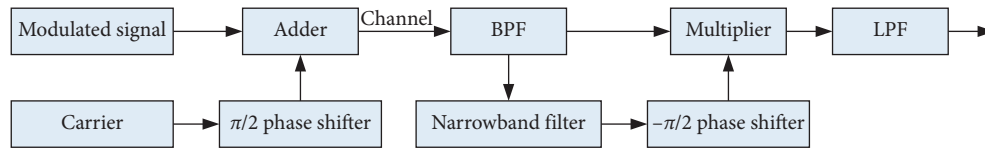


FIGURE 1: Carrier insertion method system.

baseband shaped by a baseband shaping filter. At the same time, to achieve the transmission purpose of no intersymbol interference, a matching filter is added at the receiving end [28]. The receiver sends the received data into the matched filter and uses the matched filtered data for frame synchronization. The frame synchronization information is divided into two parts. The training sequence pilot head is used to complete channel estimation. The data segment and the output of the channel estimation module are used to realize channel equalization. The output data of the equalizer is demodulated and decoded by fountain code multiuser likelihood ratio iterative detection, and finally, the received data can be obtained [29, 30].

3. System Test

3.1. System Indicators. The performance index of the UAV data link jamming environment simulator is shown in Table 1. The hardware platform design of the jamming environment simulator needs to comprehensively consider the interference environment model adopted by the UAV data link system and the implementation complexity of the real-time simulation method [31]. In the dynamic flight scene and human interference coexistence environment, the simulator should not only simulate the aviation wireless channel in different scenarios, mainly including path loss, shadow fading, multipath fading, and channel noise, but also simulate different interference patterns in real time [32–34].

3.2. Signal Acquisition. This paper simulates the functions in the original data link communication system through the multicore and multithreading in the Linux operating system and uses the TFT screen to display the data communication process in the multicore and multithreading design scheme [35]. In order to ensure that the communication data transmitted by the operating system through the serial port can be displayed on the TFT screen in real time without delay, it is necessary to test the maximum refresh rate of the TFT screen to determine whether TFT flat can be used as a display of the real-time communication process [36]. The UAV adopts downlink operation mode to transmit telemetry information such as attitude and orientation and response information of the aircraft down. The Earth station adopts the uplink operation mode to upload the inquiry control information of the Earth station; the repeater station adopts the relay operation mode to forward the down-transmitted information of the UAV to the ground station and the uploaded information of the ground station to the UAV [37].

3.3. Data Link Risk Assessment Model. When evaluating and scoring the evaluation indicators, it must be carried out in accordance with certain standards. However, most of the indicators cannot be directly assessed quantitatively only through certain specific values. This article mainly uses the AHP method to analyze the weight of the index [38].

3.4. Data Link Transceiver Equipment Test. The ground test is to select the open view conditions, assemble the airborne terminal on the UAV, fix the UAV on the off-road vehicle, and keep it connected to the flight control system. In addition, in order to observe the status of the drone, a monitoring cable is drawn from the flight control system to the computer for on-site monitoring [39]. The purpose of this operation is to simulate the working condition of the data link during the flight movement of the UAV. It is verified by a system-level simulation platform [40].

3.5. Interference Performance Test. Based on FPGA platform characteristics and clock source frequency setting, each hop differential frequency-hopping signal is processed by FFT 5 times. In the simulation, the user information is generated by the random code generator and then distributed to each branch through the serial-to-parallel conversion (S/P). The spread spectrum processing is completed in each branch through the long-code spread spectrum method and is modulated to different carriers in the way of BPSK to form the transmission signal. The signal passes through the Gaussian white noise channel and adds a certain frequency offset noise to reach the receiving end; the receiver adopts correlation demodulation, and after despreading, the BER is counted [40].

4. System Test Results

4.1. Real-Time Analysis. When the arrival rate and service time of input traffic are different, comparative experiments are carried out from four aspects: bandwidth, loss rate, queue length per unit time, and queue delay. The queue loss rate is shown in Table 2. The performance of the algorithm is shown in Figure 2. In terms of bandwidth allocation, the bandwidth of this algorithm is close to the actual bandwidth, which can well meet the output requirements of each queue. The rationality of bandwidth allocation is close to the WRR algorithm and far better than RR and SP algorithms. In terms of queue loss rate, this algorithm has the lowest queue loss rate. When the RR algorithm is used, the loss rate of queue 4 is 12.09%, and that of queue 3 is higher than 5%. When the SP algorithm is used, the loss rate of queue 4 is 23.93%. When the WRR algorithm is used, all queues are

TABLE 1: Performance indicators of UAV data link interference environment simulator.

Performance parameter	Technical index
Data link signal to be tested	Carrier frequency 70 MHz; bandwidth 10 MHz
External interference source input	Carrier frequency 70 MHz; bandwidth 10 MHz
Dry letter ratio	-20 dB~20 dB
Resolution	2 dB
Built-in noise source type	Gauss
Signal-to-noise ratio	-20 dB~40 dB; resolution 0.1 dB
Channel type	No fading, Rayleigh, rice
Channel status update rate	2 ms, 10 ms, 50 ms, 200 ms
Path loss	0~84 dB; resolution 1 dB

TABLE 2: Queue loss rate.

Loss rate (%)	Queue 1	Queue 2	Queue 3	Queue 4
RR	0	0.11	5.75	12.09
SP	0	0.49	2.21	23.93
WRR	0.99	1.85	1.81	2.88
This article	0.03	0.49	0.56	0.7

lost, but they are controlled within 3%. With this algorithm, the loss rate of each queue is controlled within 1%. As far as the queue length is concerned, both the WRR algorithm and this algorithm can control each queue to maintain a relatively equal length, while other algorithms have different queue lengths, which can easily cause some queue data to lose data due to timeout or overlength. As for queue delay, the WRR algorithm and this algorithm have more fair-queue delay, while the RR algorithm and SP algorithm have a lower delay with higher priority, and lower priority has a higher delay.

Considering that in the airborne data link system, there will inevitably be a lot of noise and various interferences during information transmission, so there is no need to consider the problem of wrong leveling. Therefore, this article mainly studies and simulates the PCCC-type Turbo code. For the data requirements in the data chain, the 1/3 code rate is adopted in the realization scheme. At the same time, considering that the block interleaver is easy to implement in hardware, in order to reduce the complexity in iterative decoding, this paper uses block interleaving as the inner interleaving of Turbo codes. The influence of the change in the number of carriers on system performance is shown in Figure 3. In the absence of frequency offset, when the number of carriers increases, the bit error rate will increase slightly. This is because when the number of carriers increases, the ISI of other carriers on each subcarrier will increase, but because the receiver works in an ideal state, its impact on the bit error rate is not too obvious. It can be seen from the figure that when there is a frequency offset, the bit error rate of the system has been significantly improved. But in the vicinity of 10db, the bit error rate can still reach 10^{-4} . With the increase of RS code redundancy, the coding efficiency is decreasing, and its realization becomes more complicated, and for any real-time communication, the bandwidth must be expanded. That is to say, the improvement of error correction performance comes at the cost of increasing bandwidth.

The comparison results of acquisition time of serial sliding correlation and variable step synchronous acquisition method under 31 symbol offsets are shown in Table 3. The time for the two methods to complete a sliding calculation is basically the same, and the variable step length takes longer time in the decision module than the sliding correlation method. Because the average sliding times are less than the sliding correlation method, the synchronous acquisition time of the variable step method is less than that of the sliding correlation method. With the increase of the number of symbol offsets, the total step size gradually decreases, which can verify the correctness of the variable step size decision method. When the number of symbol offsets between the local signal and the received signal is small, the acquisition time of serial sliding correlation is less than that of variable step size, which is mainly due to the fact that the two methods occupy too much time to the decision module; when the symbol offset of local signal and received signal is greater than 7, the acquisition time of variable step length is less than that of serial sliding correlation. This is mainly due to the large difference in the number of sliding times, and the impact of the module decision time on the overall acquisition time is small, and with the increase of the number of symbol offsets, the synchronous acquisition method with variable step size has better performance.

The synthetic test simulation result of differential frequency-hopping signal is shown as in Figure 4. It can be seen from the figure that the differential frequency-hopping signal generation module is driven by a clock with a sampling frequency of 100 MHz. When the reset signal is invalid, the residence time of each hop of the generated signal is 200 μ s, which verifies the hopping of the differential frequency-hopping signal. The speed is 5000 hop/S, which also shows that the generated differential frequency-hopping signal is correct. In the designed differential frequency-hopping bandwidth, it can be clearly seen that it is a differential frequency-hopping signal with 16 frequency points, with a carrier center frequency of 6 MHz and a bandwidth of 2.4 MHz, thus verifying the correctness of the differential frequency-hopping signal.

4.2. Antijamming Performance Analysis. In the range of SNR 15 and the number of transmit and receive antennas from 1 to 10, this paper compares the average decoding time performance of MIMO-OFDM spherical equalization

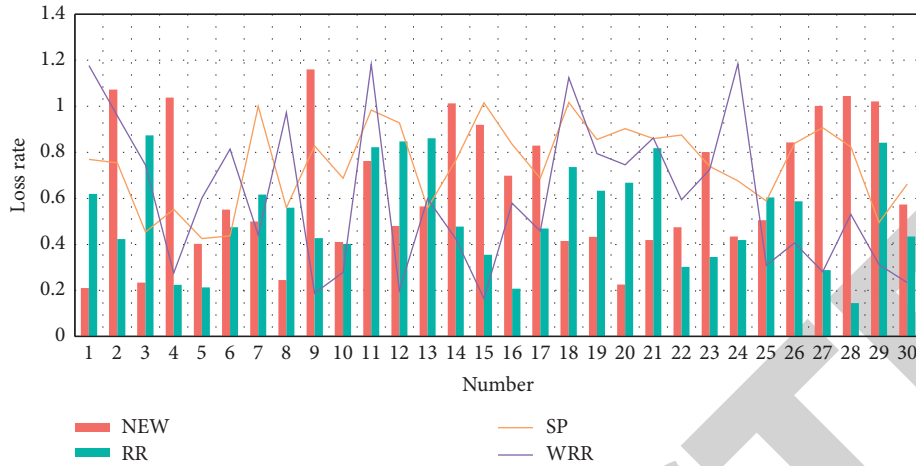


FIGURE 2: Algorithm performance.

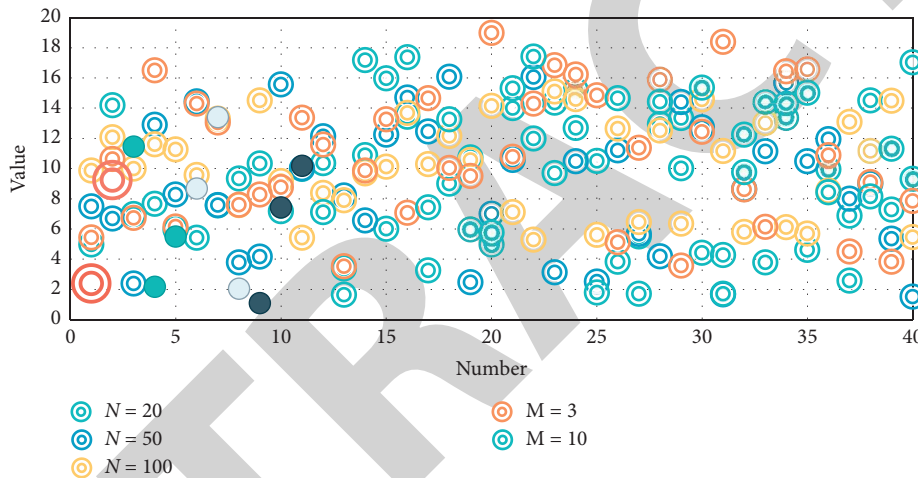


FIGURE 3: The impact of changes in the number of carriers on system performance.

TABLE 3: Comparison of capture time.

	Calculation (s)	Verdict (s)	Once (s)	All (s)
Variable step size	0.000319	0.000878	0.000929	0.010526
Sliding related	0.000107	0.000595	0.000594	0.018308

technology after external joint optimization and that of MIMO-OFDM spherical equalization technology after internal collaborative optimization. Each technology is cycled 10 times, and the performance curve of the simulation experiment is shown in Figure 5. It can be seen from the figure that the average decoding time of the two technologies increases linearly with the increase of the number of transmit and receive antennas, and the average single decoding time of MIMO-OFDM spherical equalization technology after external joint optimization is approximately 1/2 of that of the MIMO-OFDM spherical equalization technology after internal cooptimization. Due to the introduction of microcomputing and GA, the MIMO-OFDM spherical equalization technology after external joint

optimization can maintain the optimal BER performance of MIMO-OFDM spherical equalization technology after internal collaborative optimization, enhance the robustness, reduce the computational complexity, and greatly reduce the average decoding time.

The TU-6 fading channel model is shown in Table 4. The average BER of the two technologies shows a parabolic downward trend with the increase of SNR, and the low-complexity SC-FDESC-CPM technology has basically reached a BER of 0 when the SNR is about 19. The innovative equalization technology route combining SC-FDE technology and SC-CPM technology enables the UAV wireless image transmission data link system to greatly enhance the ability to resist multipath interference while fully improving bandwidth resource utilization. In order to ensure better spurious performance, a narrower bandwidth must be selected. And we choose the DDS output frequency reasonably to avoid the high spurious frequency points, so as to get better spurious performance.

The performance of the Nakagami Fading channel is shown in Figure 6. When other conditions are the same, the performance of convolutional codes in fading channels is

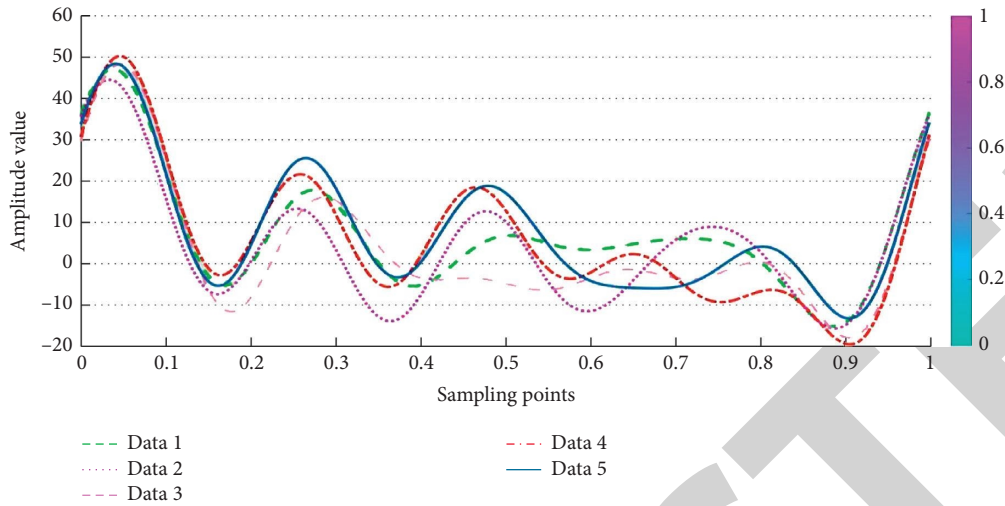


FIGURE 4: Comprehensive test simulation results generated by differential frequency-hopping signal.

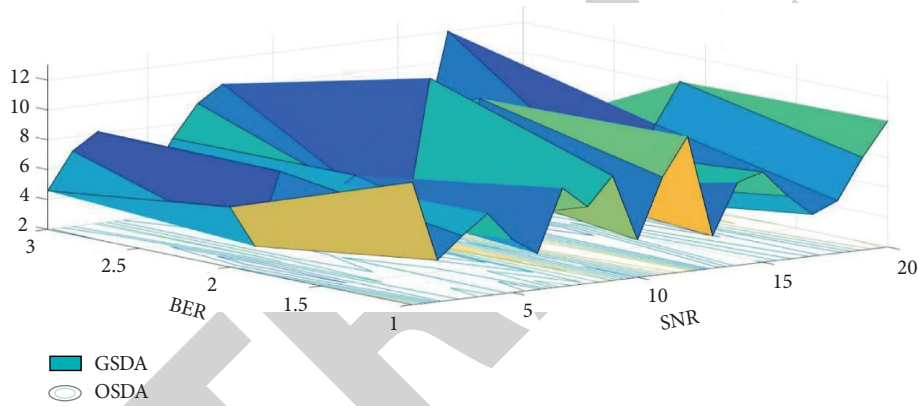


FIGURE 5: Simulation experiment results.

TABLE 4: TU-6 fading channel model.

Channel delay	Normalized power
0	0.189
1	0.379
2	0.255
8	0.090
12	0.055
25	0.032

worse than that in Gaussian white channels under the same SNR, and the smaller the m value, the worse the performance of convolutional codes. Compared with RS code, convolutional code has stronger anti-interference ability, and its encoder and decoder have a simple structure, short decoding delay, and strong random error correction ability. Therefore, the CDL and TCDL tactical common data link use convolutional code to encode the information channel, so as to improve the antijamming ability of information transmission. The message delay in the system is directly proportional to the number of messages generated per unit time and also directly related to the rationality of slot allocation. When the number of instantaneous messages exceeds the capacity of

network transmission, the message delay will be greatly increased, and the instantaneous number of messages is directly related to the simulation scenario. When the capacity of a single network cannot meet the delay requirements of the system, the number of stack networks can be increased by stacking to improve the overall capacity of the system and reduce the delay index.

4.3. Sensitivity Test Results. In the experiment, 6000 packets are tested at different distances, and a point is taken for every 20 packets. The total delay of the system is shown in Figure 7. When the distance between the UAV and base station is 200 m, the average value of total system delay is 37.5 ms. When the distance between the UAV and base station is 400 m, the average value of total system delay is about 39 ms. When the distance between the UAV and base station is 1 km, the average value of total system delay is about 43 ms. For an unmanned helicopter system, as long as the system delay is less than 80 ms under manual control, it can meet the control requirements. At different distances, the frame loss rate of the data link is different. The frame loss rate is about 1% in the range of 500 m, 2.3% in the range of 2 km,

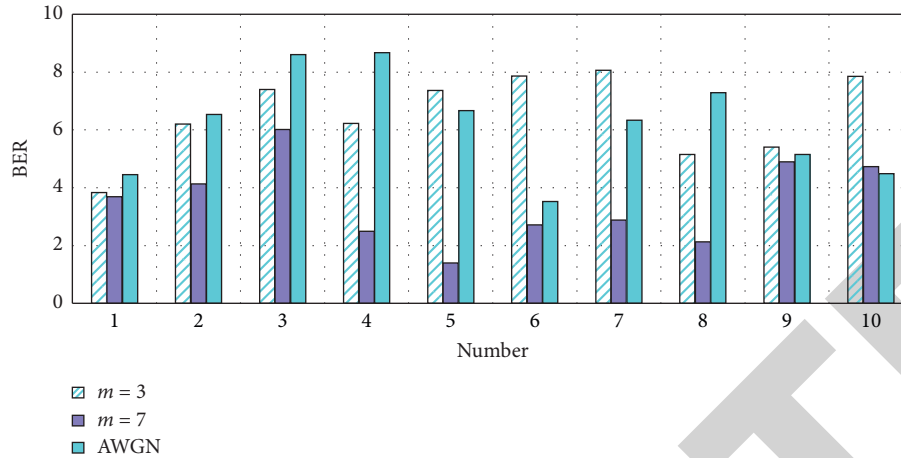


FIGURE 6: Nakagami fading channel performance.

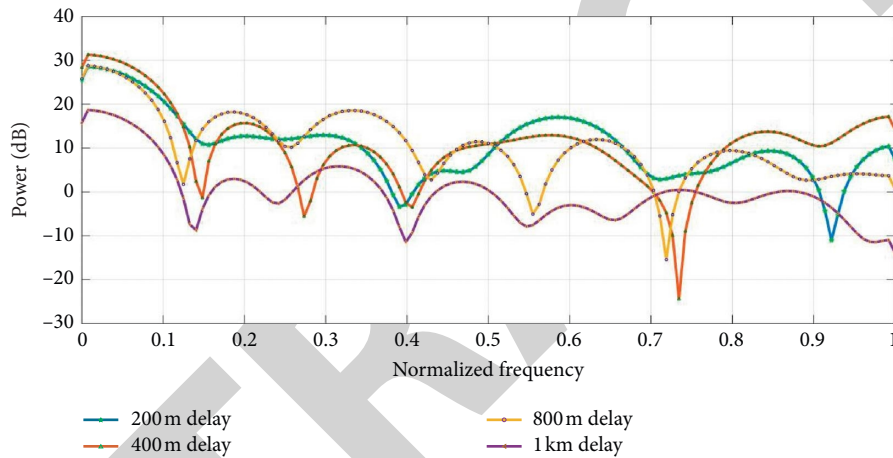


FIGURE 7: Delay curves at different distances.

and 4.5% in the range of 4 km. In the actual system, the uplink frequency is 30 Hz; for real-time remote control, the frame loss rate less than 10% has no effect.

Different frequency offset signal capture and tracking test results are shown in Figure 8. For the uplink measurement and control receiving channel, it is necessary to comprehensively verify its capture and tracking performance. The first is to capture and test different Doppler frequency offsets. It is necessary to constantly adjust the carrier frequency emitted by the vector signal source to simulate possible frequency offset values. The offset needs to cover the set carrier search range. The second is to test the tracking effect. When the receiver is in a stable tracking state, we adjust the carrier frequency emitted by the signal source to simulate the external dynamic stress and observe whether the Doppler value output by the carrier tracking loop can track the change of the signal. When adjusting the carrier frequency of the signal source, the value of one adjustment cannot be too large; usually, the value of each adjustment is below 1 kHz. When the signal is tracked stably, the output data of channel I and channel Q are basically noise, which can be seen from the magnitude of the correlation value; the frequency error and phase error of the phase detector change

within a small range, and the phase error should generally be kept at within $\pm 15^\circ$; that is, if the modulus is less than 0.26, the Doppler value can track the change of the external signal. When the actual measured external signal changes at 2 KHz/s, the tracking loop can still operate normally. Simulation tests and comprehensive results show that at a global clock frequency of 40 MHz, it takes about 0.14248 ms to complete the equalization processing of every 1024 received data, and the ideal peak throughput rate can reach 115 Mbits/s. The maximum clock is 343.595 MHz, which takes fewer resources.

TCM-4CPM demodulation hardware implementation resource occupancy is shown in Table 5. From the output spurious test results of the power amplifier, it can be concluded that the output spurious of each power amplifier unit is less than -50 dBm, the spurious suppression of each power amplifier is better than -50 dBc, and the spurious suppression of the power amplifier unit can meet the design index requirements.

The simulation results of the model are shown in Figure 9. When the nodes in the network send fewer packets and the bus model runs at low load, the delay data in the network is small. When the data is transmitted according to the exponential

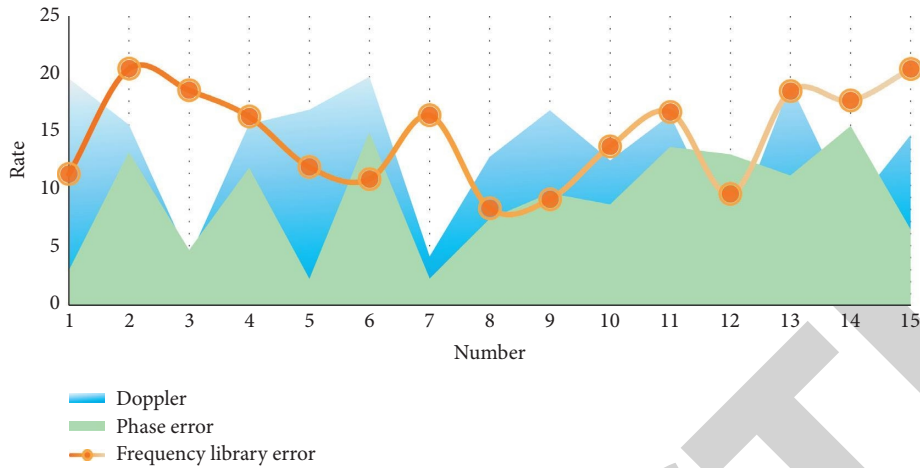


FIGURE 8: Different frequency offset signal capture and tracking test results.

TABLE 5: TCM-4CPM demodulation hardware implementation resource occupation.

Logic	Used	Available	Rate%
Registers	4737	106400	4
LUT	10911	53200	20
BLOCKRAM/FIFO	1	140	1
BUFG/BUFGCTRLs	1	32	3
DSP48 Es	3	220	1

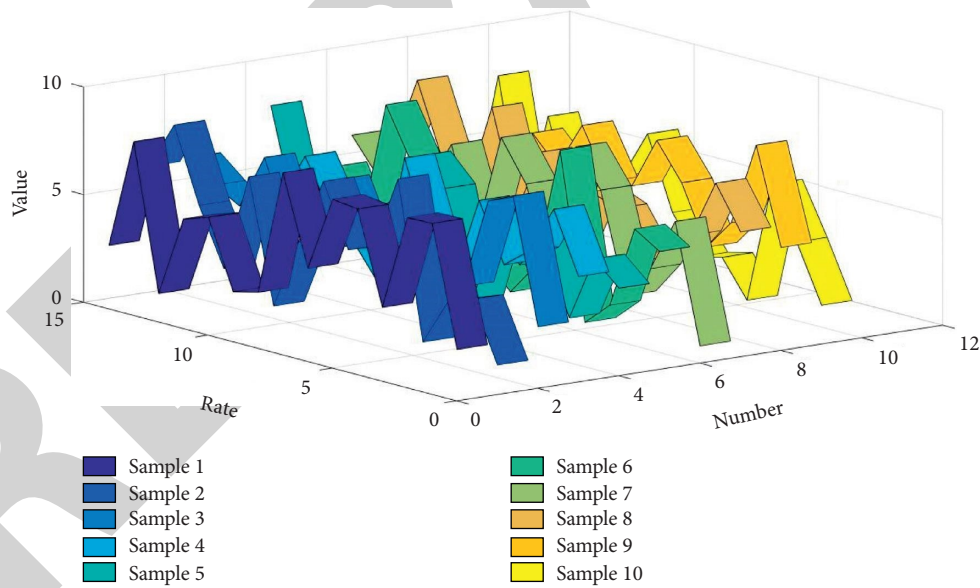


FIGURE 9: Model simulation results.

interval type, the change of network delay is not obvious, the change is not obvious, and it is maintained in a certain range. It can be seen that the real-time performance of the simulation can bus is particularly good when the network is running with low load, which meets the real-time requirements of fieldwork. Since the network is of broadcast bus type, according to the proportion of total data to the total work nodes, and considering the arbitration queue delay caused by different priorities and other factors, the received data of each work node

remains stable, which indicates that all nodes have the ability to obtain data equally, and it can be seen that the influence of network arbitration delay is small.

5. Conclusions

With the rapid development of communication technology and the increasing complexity of communication systems, a data link is widely used in the military field. Therefore, it is

more and more important to carry out modeling and simulation work on communication systems and further research on system performance evaluation. This paper mainly studies the measures to improve the real-time performance of airborne data link communication systems. From the technical model and simulation model of the communication data link system, the basic working principle is understood, the modularization analysis is carried out on the communication data link system, the functions of each module and its simulation model are sorted out, and the corresponding simulation work is carried out. It provides a solid theoretical basis for the system performance evaluation model and software design. Through the establishment of the airborne ACARS platform, the accuracy, reliability, real time, and other requirements of the system in sending downlink messages and receiving uplink messages were verified, and relevant tests were conducted under actual conditions. The results show that the system has a good message transceiving function.

Due to the difference of information processing steps on different channels, it will be out of synchronization in time, and the time delay can ensure that the information after coding is matched in time. The combat mode gradually develops from independent operation to joint operation. Therefore, the communication capacity, transmission distance, and type of transmission information are constantly expanding. In the airborne data link, due to the wide range of aircraft activities, sometimes close to the ionosphere, it is extremely easy to cause the signal to have multiple propagation paths, resulting in a multipath effect. At the same time, due to the fast-moving speed of the combat aircraft, the relative positions of the communication parties will change at a high speed, which will cause the Doppler effect.

With the development of military data communication systems against interference, the requirement of anti-interception performance is gradually improved, and the high-performance error correction algorithm is becoming more and more important in the whole system. Through the analysis of volume pick-up real-time control system request, the volume is obtained by a machine to control the system I/O response time, and the requirement of the minimum sampling period to calculate the hybrid control system of a total spool of pick-up, the I/O response time, the minimum sampling period, and the constructed hybrid bus are analyzed from the angle of real-time control system used for the feasibility of the control volume pick-up.

Data Availability

No data were used to support this study.

Conflicts of Interest

The authors declare that they have no conflicts of interest.

Acknowledgments

This work was supported in part by the Shaanxi Provincial Technology Innovation Special Project (fund), Scientific and

Technological Achievement Transfer and Promotion Plan, project number: 2020TG-002.

References

- [1] S. Wan, Z. Gu, and Q. Ni, "Cognitive computing and wireless communications on the edge for healthcare service robots," *Computer Communications*, vol. 149, pp. 99–106, 2019.
- [2] Z. Lv, "The security of internet of drones," *Computer Communications*, vol. 148, pp. 208–214, 2019.
- [3] S. N. Mohanty, E. L. Lydia, M. Elhoseny, M. Majid, G. Al Otaibi, and K. Shankar, "Deep learning with LSTM based distributed data mining model for energy efficient wireless sensor networks," *Physical Communication*, vol. 40, 2020 In press, Article ID 101097.
- [4] S. Long, M. A. Khalighi, M. Wolf, S. Bourennane, and Z. Ghassemlooy, "Investigating channel frequency selectivity in indoor visible-light communication systems," *IET Optoelectronics*, vol. 10, no. 3, pp. 80–88, 2016.
- [5] A. A. Rahmani Hosseinabadi, J. Vahidi, B. Saemi, A. Kumar Sangaiah, and M. Elhoseny, "Extended genetic algorithm for solving open-shop scheduling problem," *Soft Computing*, vol. 23, no. 13, pp. 5099–5116, 2018.
- [6] Y. Liu, H. Deng, S. Ren et al., "Peak-to-average power ratio reduction in orthogonal frequency division multiplexing-based visible light communication systems using a modified partial transmit sequence technique," *Optical Engineering*, vol. 57, no. 1, pp. 016108.1–016108.10, 2018.
- [7] P. Thakur, A. Kumar, S. Pandit, G. Singh, and S. N. Satashia, "Frameworks of non-orthogonal multiple access techniques in cognitive radio communication systems," *China Communications*, vol. 16, no. 6, pp. 129–149, 2019.
- [8] C. Li, P. Liu, C. Zou, F. Sun, J. M. Cioffi, and L. Yang, "Spectral-efficient cellular communications with coexistent one-and two-hop transmissions," *IEEE Transactions on Vehicular Technology*, vol. 65, no. 8, pp. 6765–6772, 2015.
- [9] G. Kaddoum, E. Soujeri, and Y. Nijssure, "Design of a short reference noncoherent chaos-based communication systems," *IEEE Transactions on Communications*, vol. 64, no. 2, pp. 680–689, 2016.
- [10] Y. Kyeongseok, B. Hoki, P. Kyungmi et al., "Priority based medium access control and load balancing scheme for shared situational awareness in airborne tactical data link," *The Journal of Korean Institute of Communications and Information Encees*, vol. 41, no. 10, pp. 1210–1220, 2016.
- [11] Y. Sun, D. W. K. Ng, J. Zhu, and R. Schober, "Multi-objective optimization for robust power efficient and secure full-duplex wireless communication systems," *IEEE Transactions on Wireless Communications*, vol. 15, no. 8, pp. 5511–5526, 2016.
- [12] C. X. Wang, A. Ghazal, B. Ai et al., "Channel measurements and models for high-speed train communication systems: a survey," *IEEE Communications Surveys & Tutorials*, vol. 18, no. 2, pp. 974–987, 2017.
- [13] Z. Lv, R. Lou, and K. S. Amit, "AI empowered communication systems for intelligent transportation systems," *IEEE Transactions on Intelligent Transportation Systems*, no. 99, pp. 1–9, 2020.
- [14] Q. Wang, Y. Li, and X. Liu, "Analysis of feature fatigue EEG signals based on wavelet entropy," *International Journal of Pattern Recognition and Artificial Intelligence*, vol. 32, no. 08, Article ID 1854023, 2018.
- [15] J. Zou, C. Liu, E. José, and A. Schutt, "Development of a wide-tuning-range two-parallel-plate tunable capacitor for integrated wireless communication systems," *International*

- Journal of Rf & Microwave Computer-aided Engineering*, vol. 11, no. 5, pp. 322–329, 2016.
- [16] N. Haridas and E. Elias, “Reconfigurable farrow structure-based FRM filters for wireless communication systems,” *Circuits Systems & Signal Processing*, vol. 36, no. 1, pp. 1–24, 2016.
- [17] K. Foster and D. Colombi, “Thermal response of tissue to RF exposure from canonical dipoles at frequencies for future mobile communication systems,” *Electronics Letters*, vol. 53, no. 5, pp. 360–362, 2017.
- [18] R. Bhatia, A. K. Sharma, and J. Saxena, “Improved analysis of four wave mixing with sub-plank higher-order dispersion parameters in optical communication systems,” *Optik*, vol. 127, no. 20, pp. 9474–9478, 2016.
- [19] Z. Yu, Z. Jian, Z. Yan-Yu et al., “Weight threshold check coding for dimmable indoor visible light communication systems,” *IEEE Photonics Journal*, vol. 10, no. 3, pp. 1–11, 2018.
- [20] O. S. Badarneh, “Performance evaluation of wireless communication systems over composite α - μ /Gamma fading channels,” *Wireless Personal Communications*, vol. 97, no. 4, pp. 1–15, 2017.
- [21] B. Das, M. F. L. Abdullah, B. S. Chowdhry et al., “A novel signal regeneration technique for high speed DPSK communication systems,” *Wireless Personal Communications*, vol. 96, no. 11, pp. 3249–3273, 2017.
- [22] M. Elhoseny and K. Shankar, “Optimal bilateral filter and convolutional neural network based denoising method of medical image measurements,” *Measurement*, vol. 143, pp. 125–135, 2019.
- [23] Y. Lu, X. Wang, M. D. Higgins, A. Noel, N. Neophytou, and M. S. Leeson, “Energy requirements of error correction codes in diffusion-based molecular communication systems,” *Nano Communication Networks*, vol. 11, no. 3, pp. 24–35, 2017.
- [24] B. Arif, H. Bahadir, T. Hasan et al., “Optimum transmission distance for relay-assisted free-space optical communication systems,” *Optik*, vol. 127, no. 16, pp. 6490–6497, 2016.
- [25] L. Wang, W. Chen, Z. Ding, W. Guo, and M. Peng, “Practical framework for ultra-fair dynamic interference coordination in mobile communication systems,” *IET Communications*, vol. 10, no. 4, pp. 372–380, 2016.
- [26] S. Navaratnarajah, C. Han, M. Dianati, and M. A. Imran, “Adaptive stochastic radio access selection scheme for cellular-WLAN heterogeneous communication systems,” *IET Communications*, vol. 10, no. 15, pp. 1986–1994, 2016.
- [27] Y. Morag, N. Tal, M. Nazarathy, and Y. Levron, “Thermodynamic signal-to-noise and channel capacity limits of magnetic induction sensors and communication systems,” *IEEE Sensors Journal*, vol. 16, no. 6, pp. 1575–1585, 2016.
- [28] S. Zhao, “A serial concatenation-based coding scheme for dimmable visible light communication systems,” *IEEE Communications Letters*, vol. 20, no. 10, pp. 1951–1954, 2016.
- [29] S. P. Karthi and K. Kavitha, “A survey on various reconfigurable architectures for wireless communication systems,” *International Journal of Pure and Applied Mathematics*, vol. 119, no. 12, pp. 1427–1433, 2018.
- [30] G. Kaddoum, Y. Nijsure, and H. Tran, “Generalized code index modulation technique for high-data-rate communication systems,” *IEEE Transactions on Vehicular Technology*, vol. 65, no. 9, pp. 7000–7009, 2016.
- [31] I. F. Akyildiz, P. Wang, and S.-C. Lin, “SoftWater: software-defined networking for next-generation underwater communication systems,” *Ad Hoc Networks*, vol. 46, no. 8, pp. 1–11, 2016.
- [32] C. C. Zarakovitis, Q. Ni, and J. Spiliotis, “Energy-efficient green wireless communication systems with imperfect CSI and data outage,” *IEEE Journal on Selected Areas in Communications*, vol. 34, no. 12, pp. 3108–3126, 2016.
- [33] S. Chen, S. Sun, Q. Gao et al., “Adaptive beamforming in TDD-based mobile communication systems: state of the art and 5G research directions,” *IEEE Wireless Communications*, vol. 23, no. 6, pp. 81–87, 2017.
- [34] C. Yang, Z. Yang, and Z. Deng, “Robust weighted state fusion Kalman estimators for networked systems with mixed uncertainties,” *Information Fusion*, vol. 45, pp. 246–265, 2019.
- [35] Y. Fang, G. Han, P. Chen et al., “A survey on DCSK-based communication systems and their application to UWB scenarios,” *IEEE Communications Surveys & Tutorials*, vol. 18, no. 3, pp. 1804–1837, 2017.
- [36] A. Masmoudi and T. Le-Ngoc, “Channel estimation and self-interference cancelation in full-duplex communication systems,” *IEEE Transactions on Vehicular Technology*, vol. 66, no. 1, pp. 321–334, 2017.
- [37] Z. Lv, L. Qiao, M. Shamim Hossain, and B. J. Choi, “Analysis of using blockchain to protect the privacy of drone big data,” *IEEE Network*, vol. 35, no. 1, 2020.
- [38] A. E. Abdelkareem, B. S. Sharif, and C. C. Tsimenidis, “Adaptive time varying Doppler shift compensation algorithm for OFDM-based underwater acoustic communication systems,” *Ad Hoc Networks*, vol. 45, no. 7, pp. 104–119, 2016.
- [39] Z. Lv, B. Hu, and H. Lv, “Infrastructure monitoring and operation for smart cities based on IoT system,” *IEEE Transactions on Industrial Informatics*, vol. 16, no. 3, pp. 1957–1962, 2020.
- [40] Y. Yang, Z. Zeng, J. Cheng, and C. Guo, “An enhanced DCO-OFDM scheme for dimming control in visible light communication systems,” *IEEE Photonics Journal*, vol. 8, no. 3, pp. 1–13, 2016.